MTL-Based Analysis to Distinguish High-Frequency Behavior of Interleaved Windings in Power Transformers

Makarand M. Kane and S. V. Kulkarni, *Senior Member, IEEE*

***Abstract*—An elaborate method to analyze the high-frequency behavior of transformer windings by means of the multiconductor transmission line (MTL) method is presented. A procedure for the evaluation of per-unit length parameters for transformer windings (TWs) is enumerated, which is not available in existing literature on the subject. A full-length detailed solution of the MTL method for TW is also demonstrated. A comparison of this method with the conventional circuit approach is illustrated wherever necessary. The analysis of two types of commonly used interleaved windings is performed in this paper. It is also inferred from experimental results that a conventional low-voltage impulse test is insufficient to make a distinction between the two windings. As far as inter-winding oscillations at high-frequency excitations are concerned, it also proved by the MTL analysis that one type is better than the other.**

***Index Terms*—Multiconductor transmission lines, resonances, transformer windings.**

I. Introduction

TRANSMISSION-LINE-BASED high-frequency analysis of power equipment is of interest to researchers since the 1960s [1]. Abnormal voltages with a rise time of a few nanoseconds are called very fast transient overvoltages (VFTOs) [2]. They are common in gas-insulated substations (GIS). The behavior of transformer windings (TWs) is remarkably different at high frequencies. Many times, insulation in the TW gets stressed to intolerable levels when such voltages impinge on them. These stress levels need to be considered at the design stage of a transformer. Therefore, accurate modelling of TW for waveforms containing very-high-frequency content is important [3].

Conventionally, the high-frequency behavior of TW is analyzed using an equivalent circuit approach [3], [4]. Rudenberg [1] used a transmission-line model to characterize the same behavior. The circuit model has time as the only independent variable. Hence, all voltages and currents are functions of time only. The transmission-line model has distance as another independent variable in addition to time. Therefore, the transmission-line model is midway between the circuit model and the field model (the field model has three distance variables in addition to the time variable). Recently, the MTL approach has been explored to analyze the high-frequency behavior of TW and is shown to work over a large frequency range [5]–[7]. Naderi *et al.* [8] have also proposed a hybrid model which is valid for a wide frequency band ranging from a few hundreds of kilohertz to a few tens of megahertz. A comparison between the circuit and transmission-line models is presented in [7] which reports that the latter is better when we want to analyze windings for frequencies beyond 1 MHz. An approach commonly used in the MTL methodology is to first find the solution in the frequency domain [5]–[9] and then obtain the time-domain solution by using its inverse Laplace transform. Some researchers have used the FDTD method to determine the time-domain solution [10], [11], while some others have used the discretized transmission-line model [12] and vector fitting [13].

This paper discusses the MTL method to analyze the high-frequency behavior of TW. Section II is dedicated to per-unit length parameter calculations. Very few papers have exclusively considered this aspect [14], [15]. Also, interleaved windings, proposed by Nuys [16], are used for the first time as a test object for the MTL analysis. Previous papers consider either ordinary disk windings or interleaved windings proposed by Stearn [17]. A comparison of the two types of interleaved windings is carried out to demonstrate the applicability of the MTL method.

Interleaved windings were proposed by Stearn *et al.* [17] to improve the transient response of TW. The series capacitance of interleaved windings is more than that of noninterleaved windings. This helps to improve the transient response and, therefore, the strength of the windings against voltage surges [3]. A new type of interleaved winding was later proposed by Nuys [16]. It was claimed to have a better surge response than the Stearn winding [17]. At high frequencies, the Nuys winding responds with fewer interdisk voltages than the Stearn winding. However, the explanation given by Nuys for the observed differences was qualitative and based on the difference in the magnetic couplings associated with two strands interleaved in each disk pair. Later, Teranishi [18] analyzed the windings and reported that the difference in magnetic couplings is caused by a second harmonic spatial component. Since then, no quantitative explanation has been given to distinguish the performance of these two windings. MTL-based analysis of the two types of windings is performed, and the results are compared in this paper. This study is also relevant to the context of understanding the response of windings to VFTOs.

The first section of this paper deals with accurate determination of parameter matrices ($\mathbf{R}$, $\mathbf{L}$, $\mathbf{C}$, and $\mathbf{G}$) and the second section elaborates the *full* solution in the frequency domain (not just

Manuscript received September 30, 2012; revised February 17, 2013 and May 13, 2013; accepted May 27, 2013. Date of publication July 09, 2013; date of current version September 19, 2013. Paper no. TPWRD-01035-2012.

M. M. Kane is with the research centre at TATA Motors Ltd., Pune, Maharashtra 411018, India (e-mail: mak.kane@gmail.com).

S. V. Kulkarni is with the Electrical Engineering Department, IIT Bombay, Mumbai, Maharashtra 400076, India (e-mail: svk@ee.iitb.ac.in).

Color versions of one or more of the figures in this paper are available online at http://ieeexplore.ieee.org.

Digital Object Identifier 10.1109/TPWRD.2013.2268982

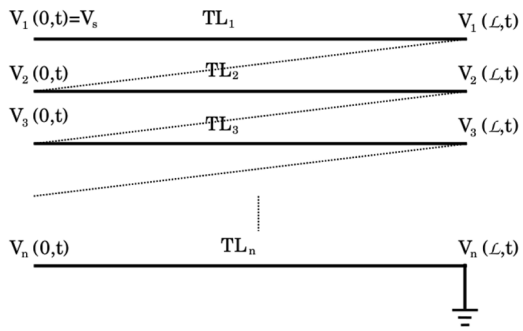

Fig. 1. MTL model of the transformer windings.

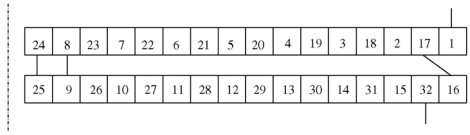

Fig. 2. Schematic of the Nuys winding disk pair.

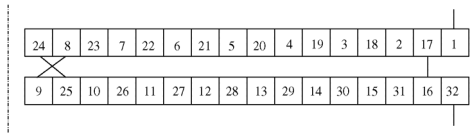

Fig. 3. Schematic of the Stearn winding disk pair.

at terminals as done in the existing literature). A solution is also obtained by using *chain parameters*, which is then compared with the full solution. For the analysis of VFTOs, a time-domain solution is also necessary. Section IV presents the solution of the MTL model in the time domain. For simplicity, a lossless model is considered and it is solved using SPICE software. In particular, the response of the model to a step wave with different rise times is studied. The last section has two parts. In the first part, experimental results illustrate that a mere impulse test is insufficient to differentiate between the two types of interleaved windings. The second part contains a comparison of the two windings by the MTL analysis.

II. Modelling and Parameter Determination

A. Modelling TW as MTL

MTL is a system of $n+1$ conductors, with one of the conductors considered as its reference conductor. In the MTL model of TW, the constituent lines are connected in series, as shown in Fig. 1. Each TL_i is a transmission line which represents a section of TW. Here, $\mathcal{L}$ is the length of each transmission line. There are two types of modelling approaches depending on what is considered as a section [7].

- Group-based model: A group of turns (it might be a disk or a layer) is considered as a single transmission line.
- Turn-based model: Each of the individual turns is modelled as a single transmission line. This model is used for the work presented in this paper.

The test objects consist of Nuys and Stearn windings. Figs. 2 and 3 show schematic representations of a disk pair of the two windings. Other details of the windings are listed in Table I. At high frequencies, the core acts as a shield [1], [8]. Hence, the core in the test object is removed and an aluminium foil of 1-mm thickness is used instead. This grounded foil, which emulates effects of the core at high frequencies, is taken as the reference conductor. At frequencies below 1 MHz, eddy currents in the core may affect actual TW response. However, the focus of this paper is mainly very high frequencies and, hence, this effect does not affect the results of interest.

B. Per-Unit Length Parameters

1) Resistance and Inductance Matrices-$\mathbf{R}$ *and* $\mathbf{L}$*:* Since the $n\times n$ matrix ($\mathbf{R}$) is used to analyze a system of $n+1$ conductors, the resistance of the reference conductor (the LV winding in this case) is added to the resistance of each conductor. This makes $\mathbf{R}$ a full matrix [19]. The $n \times n$ inductance matrix ($\mathbf{L}$) consists of self inductances as diagonal elements and mutual inductances as offdiagonal elements. There are two methods to determine these matrices:

TABLE I
Details of Sample Windings

Number of turns	128
Number of disks	8
Number of turns per disk	16
Number of spacers ID/OD	12/12
Bare conductor dimensions	12.5×2 mm
Total paper insulation	1 mm
Inside diameter	700 mm
Outside diameter	798 mm
Distance between disks	6 mm
Spacer width	55 mm
Axial height	150 mm
Relative permittivity of paper insulation ϵ_p	3.8
Relative permittivity of press-board ϵ_{pb}	4.4

1) Method 1: Here, the matrices are evaluated by time harmonic finite-element method (FEM) analysis at individual frequencies. In order to accurately take into account skin and proximity effects, the mesh needs to be refined for each higher frequency. Thus, the mesh size becomes too small. This increases the computational burden involved—the simulation time for a single frequency ranges from 4 h for a few kilohertz to 6 h for frequencies in the megahertz range.
2) Method 2: Here, the matrices are evaluated in two steps. First, magnetostatic FEM analysis is used to evaluate the external inductance matrix $\mathbf{L}$, which represents effects of fields external to conductors [19]. Then, the skin and proximity effects are taken into account by the analytical formula

$$\mathbf{Z} = \mathbf{Z}_i(\omega) + j\omega\mathbf{L} \tag{1a}$$

$$\mathbf{Z}_i(\omega) = \mathbf{A} + \mathbf{B}\sqrt{j\omega} \tag{1b}$$

where

$$\mathbf{A}_{ii} = r_{\mathrm{dc}} = \frac{1}{\sigma w t} \tag{1c}$$

and

$$\mathbf{B}_{ii} = \frac{1}{2(t+w)}\sqrt{\frac{\mu}{\sigma}}. \tag{1d}$$

Here, t and w are the thickness and width of the rectangular

conductors, ω is the angular frequency, whereas σ is the conductivity of copper.

2) Capacitance and Conductance Matrices-$\mathbf{C}$ and $\mathbf{G}$: $\mathbf{C}$ is Maxwell's capacitance matrix [19], [20]. It relates the charge per-unit length on a conductor to voltages of all other conductors. Any offdiagonal element c_{ij} can be determined in the following manner:

1) Assign a voltage level of 1 V with reference to the ground to the ith conductor. This will correspondingly have some positive charge on it.
2) Each of the remaining conductors will take some negative charge so that the system is charged neutral. If the charge on the jth conductor is $-q_j$, then

$$c_{ij} = \frac{-q_j}{V_i}. \tag{2}$$

And the ith diagonal entry is

$$c_{ii} = -\sum_{\substack{k=1\\k\neq i}}^{n} c_{ik} + c_{i0}. \tag{3}$$

Thus, $\mathbf{C}$ will be

$$\mathbf{C} = \begin{bmatrix} \sum_{k=1}^{n} c_{1k} & -c_{12} & \cdots & -c_{1n} \\ -c_{21} & \sum_{k=1}^{n} c_{2k} & \cdots & -c_{2n} \\ \vdots & \vdots & \ddots & \vdots \\ -c_{n1} & -c_{n2} & \cdots & \sum_{k=1}^{n} c_{nk} \end{bmatrix}. \tag{4}$$

Conductance matrix $\mathbf{G}$, in case of TW, contains the conductance of its insulation system (i.e., paper, oil, and pressboard). It is determined using $\mathbf{C}$ as [2], [5], and [9]

$$\mathbf{G} = \omega \mathbf{C} \tan\delta \tag{5}$$

where $\tan\delta$ is the dielectric loss tangent and $\omega = 2\pi f$.

The FEM package Maxwell is used to evaluate parameter matrices. The results given by Maxwell are lumped values for a complete turn. Per-unit length values are therefore calculated as

$$W_i^{\text{pul}} = \frac{W_i^{\text{lumped}}}{\mathcal{L}_i} \tag{6}$$

$$W_{ij}^{\text{pul}} = \frac{2W_{ij}^{\text{lumped}}}{\mathcal{L}_i + \mathcal{L}_j} \tag{7}$$

where W represents an element of the parameter matrices, "pul" stands for per unit length, and $\mathcal{L}$ represents the turn length. Subscripts i and j denote the ith line and jth line, respectively.

These parameter matrices are incorporated in further analysis.

III. Solution of the MTL Model in Frequency Domain

MTL equations in the frequency domain are [19]

$$\frac{d\overline{\mathbf{V}}(x)}{dx} = -\overline{\mathbf{Z}}\overline{\mathbf{I}}(x) \tag{8a}$$

$$\frac{d\overline{\mathbf{I}}(x)}{dx} = -\overline{\mathbf{Y}}\overline{\mathbf{V}}(x) \tag{8b}$$

where

$$\overline{\mathbf{Z}} = \mathbf{R} + j\omega\mathbf{L} \tag{9a}$$

$$\overline{\mathbf{Y}} = \mathbf{G} + j\omega\mathbf{C}. \tag{9b}$$

The variables with bars in (8) and (9) are phasors. Hereafter, the bars will be dropped for convenience. Equations (8) are solved by decoupling them using a transformation matrix $\mathbf{T}$. The decoupled lines are then referred to as modes. Hence, for an n-conductor MTL, there are n-independent modal lines. The voltages $\mathbf{V}$ and the currents $\mathbf{I}$ can then be expressed as a linear combination of these modes as follows:

$$\mathbf{V}(x) = \mathbf{Y}^{-1}\mathbf{T}\boldsymbol{\gamma}\left(\mathbf{e}^{-\boldsymbol{\gamma}x}\mathbf{I}_m^{+} + \mathbf{e}^{\boldsymbol{\gamma}x}\mathbf{I}_m^{-}\right) \tag{10a}$$

$$\mathbf{I}(x) = \mathbf{T}\left(\mathbf{e}^{-\boldsymbol{\gamma}x}\mathbf{I}_m^{+} - \mathbf{e}^{\boldsymbol{\gamma}x}\mathbf{I}_m^{-}\right) \tag{10b}$$

where $\mathbf{T}$ is the diagonalizing matrix for $\mathbf{YZ}$; $\boldsymbol{\gamma}^2 = \mathbf{T}^{-1}\mathbf{YZT}$; $\mathbf{I}_m^{+}$ is the forward propagating component of modal current; and $\mathbf{I}_m^{-}$ is the backward propagating component of modal current.

A. Solution Specific to the MTL Model of TW

Appropriate boundary conditions are required to find $\mathbf{I}_m$s in (10). These can be obtained by looking at the setup in Fig. 1 as

$$V_i(\mathcal{L}) = V_{i+1}(0) \qquad i = 1, 2, \ldots, n-1 \tag{11a}$$

$$I_i(\mathcal{L}) = I_{i+1}(0) \qquad i = 1, 2, \ldots, n-1 \tag{11b}$$

$$V_1(0) = V_s \tag{11c}$$

$$V_n(\mathcal{L}) = 0. \tag{11d}$$

Here, V_s is the applied voltage between the start and end of the winding. Equation (11) gives $2n$ boundary conditions which can be used to solve $2n$ unknowns in (10). They can be solved to obtain the full solution in the frequency domain.

Equation (10) gives $\mathbf{V}$ and $\mathbf{I}$ at one frequency. The solution over the entire frequency spectrum is deduced by sweeping the frequency. It should also be noted that here the currents and voltages are functions of x, where x varies from 0 to $\mathcal{L}$. Hence, this is called the full solution and $\mathbf{V}$, thus obtained, is useful to find exact locations of intolerable interwinding voltages, if any.

B. Solution Using the Chain Parameter Matrix

The chain parameter matrix (CHPM) relates the voltages and currents between any two points x_1 and x_2 on an MTL [19]. The equations appear as follows:

$$\begin{bmatrix} \mathbf{V}(x_2) \\ \mathbf{I}(x_2) \end{bmatrix} = \begin{bmatrix} \boldsymbol{\Phi}_{11}(x_2 - x_1) & \boldsymbol{\Phi}_{12}(x_2 - x_1) \\ \boldsymbol{\Phi}_{21}(x_2 - x_1) & \boldsymbol{\Phi}_{22}(x_2 - x_1) \end{bmatrix} \begin{bmatrix} \mathbf{V}(x_1) \\ \mathbf{I}(x_1) \end{bmatrix}. \tag{12}$$

Putting $x_2 = \mathcal{L}$ and $x_1 = 0$, we obtain the elements of CHPM as [19]

$$\boldsymbol{\Phi}_{11}(\mathcal{L}) = \cosh(\sqrt{\mathbf{ZY}}\mathcal{L}) \tag{13a}$$

$$\boldsymbol{\Phi}_{12}(\mathcal{L}) = -\sinh(\sqrt{\mathbf{ZY}}\mathcal{L})\mathbf{Z}_c \tag{13b}$$

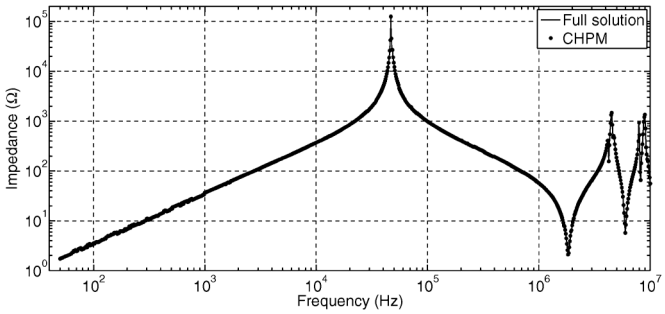

Fig. 4. Frequency-domain solution.

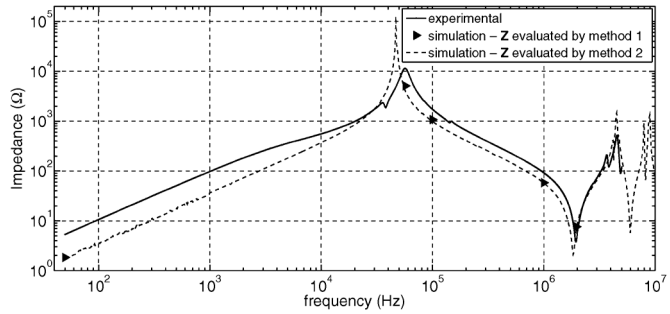

Fig. 5. Comparison of MTL model simulation and experimental results.

$$\mathbf{\Phi}_{21}(\mathcal{L}) = -\mathbf{Z}_c^{-1}\sinh(\sqrt{\mathbf{ZY}}\mathcal{L}) \tag{13c}$$

$$\mathbf{\Phi}_{22}(\mathcal{L}) = \mathbf{Y}\cosh(\sqrt{\mathbf{ZY}}\mathcal{L})\mathbf{Y}^{-1} \tag{13d}$$

where $\mathbf{Z}_c = \mathbf{ZT}\boldsymbol{\gamma}^{-1}\mathbf{T}^{-1}$ and $\sqrt{\mathbf{ZY}} = \mathbf{Y}^{-1}\mathbf{T}\boldsymbol{\gamma}\mathbf{T}^{-1}\mathbf{Y}$. It should be noted that CHPM is a $2n \times 2n$ matrix. Applying the boundary conditions given in (11) and (12) and performing some row and column operations, we can arrive at voltages and currents at the terminals of the lines, that is, $\mathbf{V}(\mathcal{L})$ and $\mathbf{I}(\mathcal{L})$. Thus, for a turn-based model, this method gives voltages and currents only at the start and end of the turns. Hereafter, it will be called the CHPM solution.

C. Measurement and Simulation Results

As discussed in Section II, Nuys and Stearn windings are the test objects in this paper. However, the discussion of results obtained for the Stearn winding is postponed until Section V.

The frequency-domain solution of the MTL model is obtained using both algorithms (full solution and CHPM solution) coded in MATLAB. The solution contains voltages and currents as functions of frequency and distance. The impedance then can be easily obtained as

$$Z = \left|\frac{V_s}{I_{V_s}}\right|. \tag{14}$$

Here, I_{V_s} is the current supplied by the source V_s (see Fig. 1). The two solutions are compared in Fig. 4. The methods give identical results. This is expected because CHPM is, in a way, the *full* solution but derived only at the terminals of the transmission line. Thus, any of the methods can be used interchangeably if we are interested only in terminal voltages and currents. Hereafter, only the detailed solution will be considered.

The results thus obtained can be verified in various ways through impedance versus frequency measurements. This is accomplished by using a Hioki-make LCR meter. Fig. 5 shows the comparison of the simulated and measured impedances. For simulation of the MTL model, the impedance matrix $\mathbf{Z}$ is obtained by both methods, outlined in Section II-B. However, method 1 is used for only a few selected frequencies due to the involved computational burden. It can be observed that $\mathbf{Z}$ values calculated from both methods are in good agreement. Hence, method 2, which is less complicated and computationally fast, is used hereafter. It should be noted that a full coil of eight disks is used for impedance versus frequency measurements. Since only two disks are modelled, the impedance Z, obtained by the simulation, is multiplied by 4 as all disks are connected in series. The simulation results are in fairly good agreement with the measured ones.

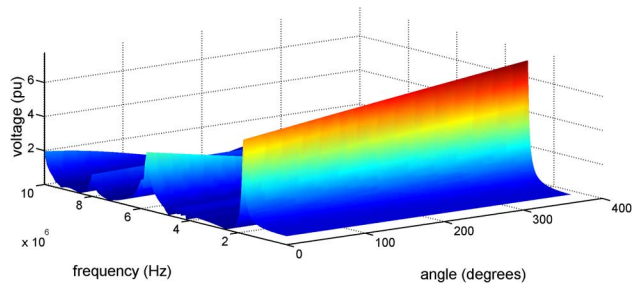

Fig. 6. Voltage distribution for the Nuys disk: interturn voltage between turn 3 and 19.

D. Voltage Distribution and Interdisk Voltages

The main advantage of the full solution is that voltage distribution over the full length of turns can be determined. In the updated work reported on the subject, parameter matrices similar to CHPM are used to obtain the voltage distribution [5], [7]–[9]. But with the full solution, a detailed plot of voltage versus frequency along length can be obtained as shown in Fig. 6. The voltage is plotted in per unit (p.u.) values with the applied voltage V_s as the base quantity. This voltage is plotted against frequency and length. One axis shows the frequency in Hertz and the other axis shows the angle in degrees. Since the lengths of turns in a disk winding are different, length is not represented in meters but in terms of degrees. Hence, the angle varies from 0 to 360°. The figure shows the voltage between the 3rd and 19th turns of the Nuys disk pair. It can be seen that the voltage reaches as high as 8 times the applied voltage at about 1 MHz. Hence, if an abnormal voltage with an appreciable magnitude at this frequency impinges on the winding, excessive interturn voltages will be developed.

IV. Solution of the MTL Model in the Time Domain

As discussed in Section I, the time-domain solution for the MTL model can be determined in various ways, such as inverse Laplace transform and FDTD. An easier way is to use a circuit simulator—SPICE—which has a model of a two-conductor line. To simplify the analysis, a lossless model of MTL was considered which can be formulated as

$$\frac{\partial \mathbf{V}}{\partial x} = -\mathbf{L}\frac{\partial \mathbf{I}}{\partial \mathbf{t}} \tag{15a}$$

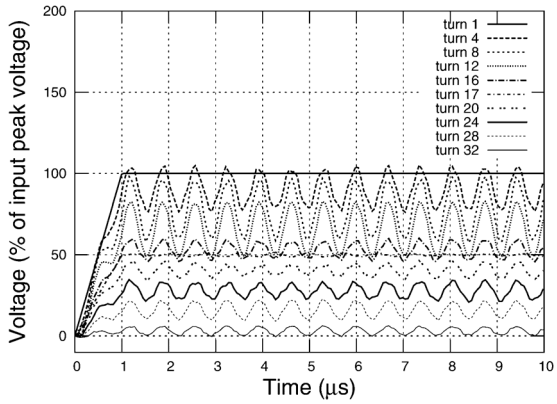

Fig. 7. Step response of the MTL model of the Nuys disk pair: rise time 1 μs.

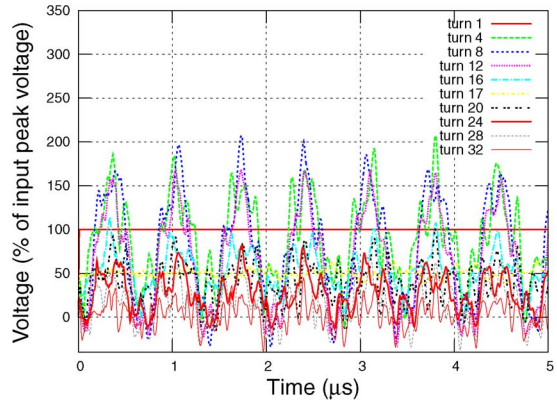

Fig. 8. Step response of the MTL model of the Nuys disk pair: rise time 0.01 μs.

$$\frac{\partial \mathbf{I}}{\partial x} = -\mathbf{C}\frac{\partial \mathbf{V}}{\partial \mathbf{t}}. \tag{15b}$$

These are coupled differential equations. Decoupling or transformation matrices $\mathbf{T_v}$ and $\mathbf{T_i}$ are determined such that they diagonalize $\mathbf{L}$ and $\mathbf{C}$ simultaneously [19]

$$\frac{\partial \mathbf{V}_m}{\partial x} = -\mathbf{T_v^{-1}}\mathbf{L}\mathbf{T_i}\frac{\partial \mathbf{I}_m}{\partial t} = \mathbf{L}_m\frac{\partial \mathbf{I}_m}{\partial t} \tag{16a}$$

$$\frac{\partial \mathbf{I}_m}{\partial x} = -\mathbf{T_i^{-1}}\mathbf{C}\mathbf{T_v}\frac{\partial \mathbf{V}_m}{\partial t} = \mathbf{C}_m\frac{\partial \mathbf{V}_m}{\partial t} \tag{16b}$$

where the subscript m refers to modal quantities. It should be noted that the modal transmission lines are independent of each other. Thus, (16) represents n standard lossless two-conductor transmission lines [19]. The actual line voltages and currents are

$$\mathbf{V} = \mathbf{T_v}\mathbf{V}_m \tag{17a}$$

$$\mathbf{I} = \mathbf{T_i}\mathbf{I}_m. \tag{17b}$$

A. Solution Specific to the Lossless MTL Model of TW

Equation (16) states that an n conductor lossless MTL can be represented in the time domain as n-decoupled two-conductor transmission lines. These lines are coupled by (17). Thus, (15) can be modelled in SPICE to obtain an exact solution of the lossless MTL model as demonstrated in [19]. It should be noted that this method provides voltages and currents only at the terminals of the line and not over its full length. However, this is a simpler way to obtain the time-domain solution. Also, as a turn-based model is employed, this solution is also fairly detailed to give accurate intersection voltages.

Out of the many SPICE variants available, LTSpice is used in this paper. The rise time of a VFTO is usually tens of nanoseconds or few microseconds. A disk pair of Nuys winding (see Fig. 2) is modelled as a lossless MTL in LTSpice. Voltages at the starting points of various turns are shown in Figs. 7 and 8 for the rise times of 1 and 0.01 μs, respectively. The figures clearly show that the less rise time of the wave, the greater the magnitude of the transient voltages within the disk pair.

B. Comparison of the MTL Model With the Circuit Model

The circuit model for the Nuys winding is shown in Fig. 9 for a 6 turns/disk case for brevity. It is the same model as proposed by Teranishi [18]. It is a lossy model; the inductances shown in the model include resistive effects. The inductances in the model are calculated by an analytical method by formulae given in [9]. The capacitances are calculated by analytical formulae given in [3]. Figs. 7 and 10 highlight that the circuit model response is more oscillatory compared to the MTL model. This might be because all interturn capacitances are not considered in the circuit model. For the rise time of 0.01 μs (see Figs. 8 and 11), it is seen that the responses of the two models are different. This reinstates the fact that as frequency increases, the interturn capacitances play an important role in deciding the response.

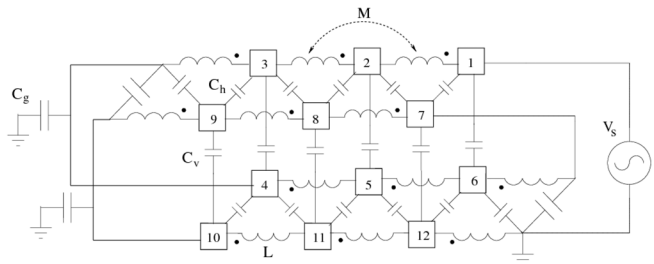

Fig. 9. Turn-based circuit model of the Nuys disk pair.

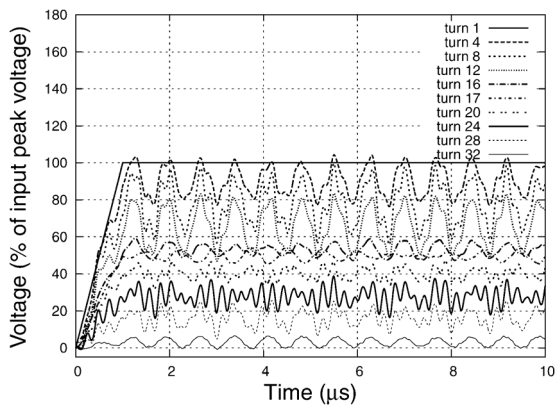

Fig. 10. Step response of the circuit model of the Nuys disk pair: rise time 1 μs.

C. Transient Voltage Distribution

Voltage distribution along TW is linear in the steady state. Voltages oscillate before reaching the linear distribution. The closer the initial voltage distribution to the final one, the better the response is to abnormal voltages [3]. This criteria will be

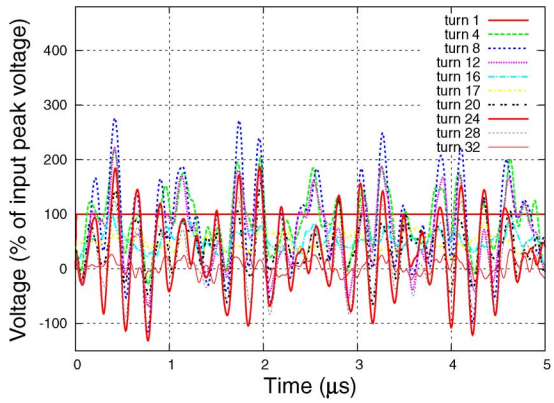

Fig. 11. Step response of the circuit model of the Nuys disk pair: rise time 0.01 μs.

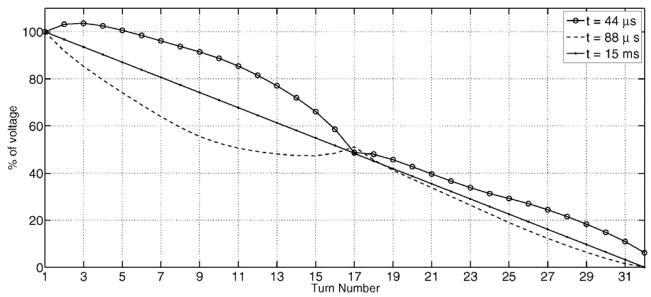

Fig. 12. Transient voltage distribution along the Nuys disk pair: MTL model.

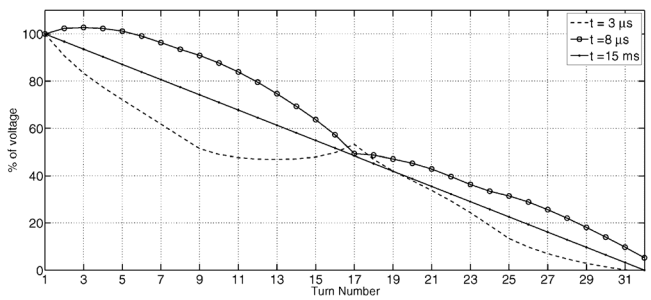

Fig. 13. Transient voltage distribution along the Nuys disk pair: circuit model.

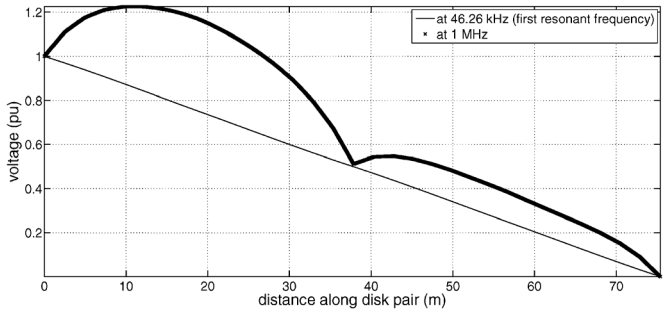

Fig. 14. Voltage distribution along the Nuys disk pair: frequency-domain solution.

TABLE II
TERMINOLOGY OF NUYS AND STEARN WINDINGS

Term used	Meaning	Example
Strand	Half of the total turns (in a disk pair) in order they appear	Turns 1 through 16
Disk	All turns in a disk in the order in which they appear	Turns 1,17,2,18,3,19,4,20,5, 21,6,22,7,23,8,24
Inner end-turns	Turns near the inner periphery	Turns 24 and 25 for Nuys winding and turns 24 and 9 for Stearn winding
Outer end-turns	Turns at the outer periphery	Turns 1 and 16 for Nuys and turns 1 and 32 for Stearn

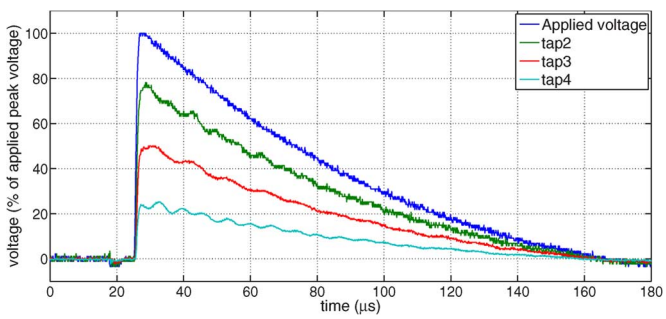

Fig. 15. Stearn winding: low-voltage impulse response.

useful while comparing Nuys and Stearn windings in the next section. Voltage distribution along the Nuys disk pair is illustrated in Figs. 12 and 13. These voltage distributions at various time instants correspond to responses to a step wave of 1-μs rise time, obtained through the MTL and circuit models.

The frequency-domain solution also gives similar distribution as can be seen in Fig. 14. The voltage distribution at the first natural frequency (corresponding to Fig. 5), which is not a very high frequency, is linear. On the contrary at 1 MHz, it is significantly nonlinear. It should be noted that these results match those reported by Teranishi [18].

V. COMPARISON OF THE NUYS AND STEARN WINDINGS

This section compares MTL solutions of Nuys and Stearn windings. In both windings (shown in Figs. 2 and 3), two disks form a unit. In the Nuys winding, the inner crossover is avoided (see turns 8, 9, 24, and 25). Table II explains the terminology that will be used to refer to various parts of the two windings.

A. Experiments on the Windings

To investigate the difference in the high-frequency behavior of the two windings, the following tests are carried out:

1) Test With Recurrent Surge Generator (RSG): This instrument generates a standard low-voltage impulse (1.2 μs/50 μs) which is applied across the windings (each consists of four disk pairs connected in series). Three taps are available for measurement, one at the end of each disk pair. Figs. 15 and 16 show that there is no difference between the response of the two windings. This underlines the fact that the distinction between Stearn and Nuys windings is not possible with standard impulse waveforms.

2) Frequency-Response Test: A Hioki-make LCR meter is used to measure impedance versus frequency characteristics

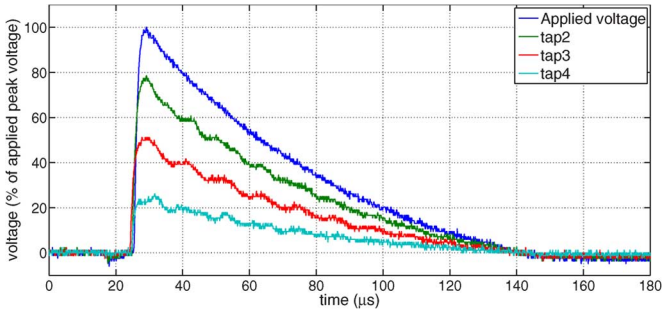

Fig. 16. Nuys winding: low-voltage impulse response.

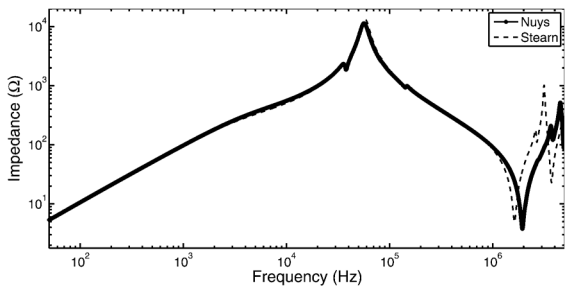

Fig. 17. Measured frequency response of the Nuys and Stearn windings.

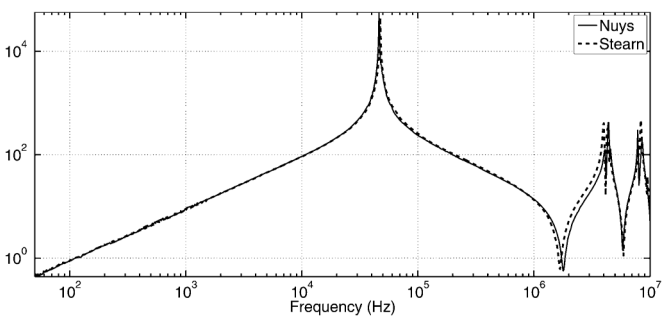

Fig. 18. Frequency response of the MTL model of the Nuys and Stearn windings.

(Fig. 17). It is clear that up to 1 MHz, the two windings exhibit no significant differences and they show some difference in the frequency band from 1 to 5 MHz. These tests confirm the fact that their responses differ only in the region of very high frequencies beyond 1 MHz.

B. MTL-Based Simulation Results

Frequency-domain simulation results of the MTL model of the Stearn winding are compared with those of the Nuys winding in Fig. 18. It illustrates that the MTL model also shows differences only in the high-frequency region. Intersection voltages can be analyzed from time-domain simulation results. The response of the Stearn disk pair for a step front of 1-μs rise time is shown in Fig. 19, which depicts the voltages at the midpoints of both disks and at the inner end turns and the outer end turns. It can be seen that the response is quite different from that of the Nuys disk pair (see Fig. 7).

Fig. 20 clearly shows the difference in the transient voltage distributions along the two types of windings for a step wave

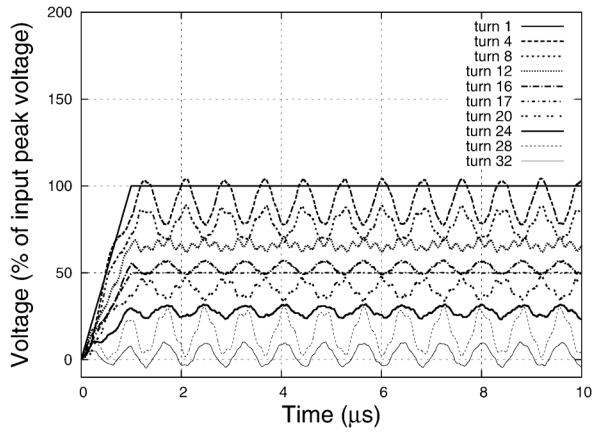

Fig. 19. Transient response of the MTL model of the Stearn disk pair: rise time 1 μs.

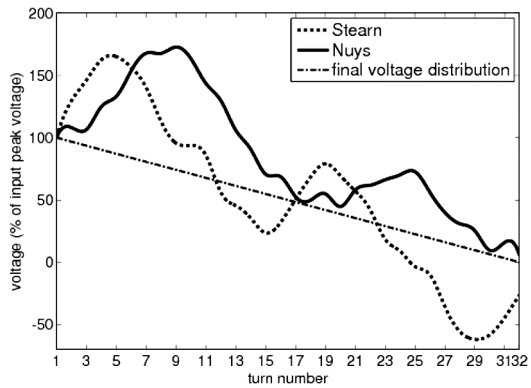

Fig. 20. Transient voltage distribution along the Nuys and Stearn windings.

of 1-ns rise time (representing a VFTO) applied across the disk pairs. The figure agrees well with [18, Fig. 8] in the sense that the voltage distribution in the Nuys winding has only two antinodes (as described in the reference) which are at the inner end turns in each disk. On the contrary, the voltage distribution in the Stearn winding has four antinodes, which are at the middle of each disk (at turns 5, 13, 20, and 28 in Fig. 3) in the disk pair. The initial voltage distributions in both windings are not close to the final one. Hence, both windings have oscillations in them.

However, the main difference is in the interdisk voltages during the transient period. In the Nuys winding, voltages of all turns oscillate together. On the contrary, in the Stearn winding, the voltages of turns 1–8 in disk 1 oscillate in the direction opposite those of the voltages of turns 9–16 in disk 2. Similarly, the voltages of turns 17–24 in disk 1 oscillate in the direction opposite those of the voltages of turns 25–32 in disk 2. This results in higher interdisk voltage differences in the Stearn winding than in the Nuys winding. Figs. 21 and 22 vividly illustrate this point. These figures show the voltage difference between the mid-level turns of the two disks in both windings (refer to Figs. 2 and 3). The maximum difference in the voltages between turns 5 and 28 for the Stearn winding goes as high as 200%. The corresponding difference for the Nuys winding is around 60%. Thus, the Nuys winding is better in responding to

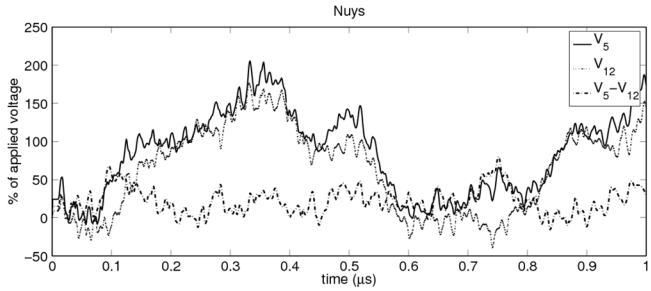

Fig. 21. Interturn voltage at the middle of the disks for the Nuys windings (response to a step voltage with a rise time of 1 ns).

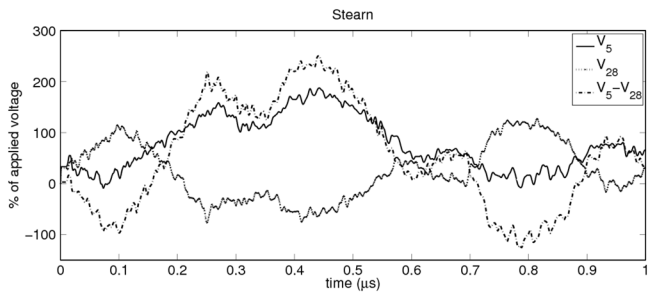

Fig. 22. Interturn voltage at the middle of the disks for the Stearn windings (response to a step voltage with a rise time of 1 ns).

very fast transient overvoltages than the Stearn winding as far as interdisk voltages are concerned.

VI. Conclusion

The MTL method is better than the conventional circuit model method for the analysis of TW at very high frequencies. However, no well-formulated and detailed procedures specific to TW are available for the MTL method. This paper has elaborated the method and illustrated calculation of per-unit length parameters. The MTL model of TW can be easily analyzed in SPICE to obtain a time-domain solution. The two solutions—one in the frequency domain and the other in the time domain—can be used to understand the complete behavior of TW to step fronted surges. There can be many applications of this method from design to diagnostics.

This paper further compares the VFTO characteristics of the Nuys and Stearn windings using the MTL method. It has been comprehensively demonstrated through simulations and measurements that the Nuys and Stearn windings respond to standard impulse voltages almost identically. However, the performance of the former is significantly better than that of the latter for VFTOs.

The contribution of the reported work is in three aspects: 1) a detailed algorithm has been presented to analyze TW using the MTL method along with an elaborate explanation of per-unit length parameter calculations; 2) MTL analysis of the Nuys winding is presented, including the corresponding full-length solution; and 3) the application of the MTL method for comparing responses of different interleaved windings is demonstrated.

Acknowledgment

The authors would like to thank Crompton Greaves Ltd., India, for providing the model coils and the RSG meter used in this paper.

References

[1] R. Rudenberg, *Electrical Shock Waves in Power Systems: Traveling Waves in Lumped and Distributed Circuit Elements*. Cambridge, MA: Harvard University Press, 1968.

[2] K. Cornick, B. Filliat, C. Kiney, and W. Muller, "Distribution of very fast transient overvoltages in transformer windings," in *CIGRE Study Committee*, 1992, vol. 12-204.

[3] S. V. Kulkarni and S. A. Khaparde, *Transformer Engineering: Design, Technology and Diagnostics*, 2nd ed. Boca Raton, FL: CRC, Sep. 2012.

[4] J. Weed and Murray, "Abnormal voltages in transformers," *Trans. AIEE*, vol. XXXIV, pp. 2197–2236, 1915.

[5] M. Popov, L. van der Sluis, R. P. P. Smeets, and J. L. Roldan, "Analysis of very fast transients in layer-type transformer windings," *IEEE Trans. Power Del.*, vol. 22, no. 1, pp. 238–247, Jan. 2007.

[6] Y. Yu and W. ZanJi, "Wide band modeling of large power transformer windings for very fast transient overvoltage (VFTO) analysis," *Sci. China Ser. E: Technol. Sci.*, vol. 52, pp. 2597–2604, 2009.

[7] S. M. H. Hosseini, M. Vakilian, and G. B. Gharehpetian, "Comparison of transformer detailed models for fast and very fast transient studies," *IEEE Trans. Power Del.*, vol. 23, no. 2, pp. 733–741, Apr. 2008.

[8] T. R. B. Mohammad, S. Naderi, M. S. Naderi, R. Ghaemmaghami, and A. Nasiri, "Determination of partial discharge propagation and location in transformer windings using a hybrid transformer model," *J. Elect. Power Compon. Syst.*, vol. 35, pp. 607–623, 2007.

[9] A. M. Jafari and A. Akbari, "Partial discharge localization in transformer windings using multi-conductor transmission line model," *Elect. Power Syst. Res.*, vol. 78, no. 6, pp. 1028–1037, 2008.

[10] Z. Zhongyuan, G. Shuguo, L. Fangcheng, and L. Yunpeng, "The calculation of the voltage distribution in transformer windings under VFTO based on FDTD method," in *Proc. IEEE Asia Pacific Conf. Circuits Syst.*, Dec. 2006, pp. 856–859.

[11] E. Agheb, E. Hashemi, A. Mousavi, and H. K. Hoidalen, "Study of very fast transient overvoltages and electric field stresses in air-cored pulsed transformers based on FDTD," in *Proc. 3rd Int. Adv. Res. Workshop Transformers*, Oct. 2010, pp. 303–308.

[12] M. Popov, R. Smeets, L. van der Sluis, H. de Herdt, and J. Declercq, "Experimental and theoretical analysis of vacuum circuit breaker prestrike effect on a transformer," *IEEE Trans. Power Del.*, vol. 24, no. 3, pp. 1266–1274, Jul. 2009.

[13] B. Gustavsen and A. Semlyen, "Simulation of transmission line transients using vector fitting and modal decomposition," *IEEE Trans. Power Del.*, vol. 13, no. 2, pp. 605–614, Apr. 1998.

[14] P. McLaren and H. Oraee, "Multiconductor transmission-line model for the line-end coil of large ac machines," *Proc. Inst. Elect. Eng., Elect. Power Appl.*, vol. 132, no. 3, pp. 149–156, May 1985.

[15] Z. Du, L. Ruan, C. Zhao, J. Ruan, Y. Wu, and T. Wang, "Calculation of electrical parameters for studies on propagation characteristic of pd along transformer winding," in *Proc. Int. Conf. Comput. Elect. Eng.*, Dec. 2008, pp. 926–931.

[16] R. van Nuys, "Interleaved high-voltage transformer windings," *IEEE Trans. Power App. Syst.*, vol. PAS-97, no. 5, pp. 1946–1954, Sep. 1978.

[17] A. Chadwick, J. Ferguson, D. Ryder, and G. Stearn, "Design of power transformers to withstand surges due to lightning, with special reference to a new type of winding," *Proc. Inst. Elect. Eng., Power Eng.*, vol. 97, no. 60, pp. 737–744, Dec. 1950.

[18] T. Teranishi, M. Ikeda, M. Honda, and T. Yanari, "Local voltage oscillation in interleaved transformer windings," *IEEE Trans. Power App. Syst.*, vol. PAS-100, no. 2, pp. 873–881, Feb. 1981.

[19] C. R. Paul, *Analysis of Multiconductor Transmission Lines*. Hoboken, NJ: Wiley, 1994.

[20] J. Canright and R. E. , "Capacitance: Relationships and measurements [for multiple conductors in VLSI packages and PWB]," in *Proc., 40th Electron. Compon. Technol. Conf.*, May 1990, vol. 1, pp. 163–168.

Makarand M. Kane was born in Chiplun, Maharashtra, India, in 1987. He received the B.Tech. degree in electrical engineering from Government College of Engineering, Pune, Maharashtra, India, in 2008 and the M.Tech. degree in power electronics and power systems from IIT Bombay, Mumbai, India, in 2011.

Currently, he is with the Engineering Research Centre, TATA Motors Ltd., Pimpri, Pune, Maharashtra, India. His research interests include computational electromagnetics, electrical machines, and transient studies.

S. V. Kulkarni (SM'08) is a Professor in the Electrical Engineering Department, Indian Institute of Technology, Bombay, India. Previously, he was with Crompton Greaves Ltd. and specialized in the design and development of transformers up to the 400-kV class. He has authored a book *Transformer Engineering: Design, Technology, and Diagnostics* (CRC/Taylor & Francis). He is the author of many professional publications in reputed journals and conferences. His research interests include analysis and diagnostics of power transformers, computational electromagnetics, and distributed generation.

Prof. Kulkarni is a recipient of the Young Engineer Award from Indian National Academy of Engineering. He also received the Career Award for Young Teachers from All India Council for Technical Education. He is a Fellow of the Indian National Academy of Engineering. Field Computation Laboratory and Insulation Diagnostics Laboratory have been established by him in his department.